Supplement of Atmos. Chem. Phys., 20, 1217–1232, 2020
https://doi.org/10.5194/acp-20-1217-2020-supplement

Atmospheric Chemistry and Physics
Open Access

Supplement of

Observationally constrained modeling of atmospheric oxidation capacity and photochemical reactivity in Shanghai, China

Jian Zhu et al.

Correspondence to: Shanshan Wang (shanshanwang@fudan.edu.cn)

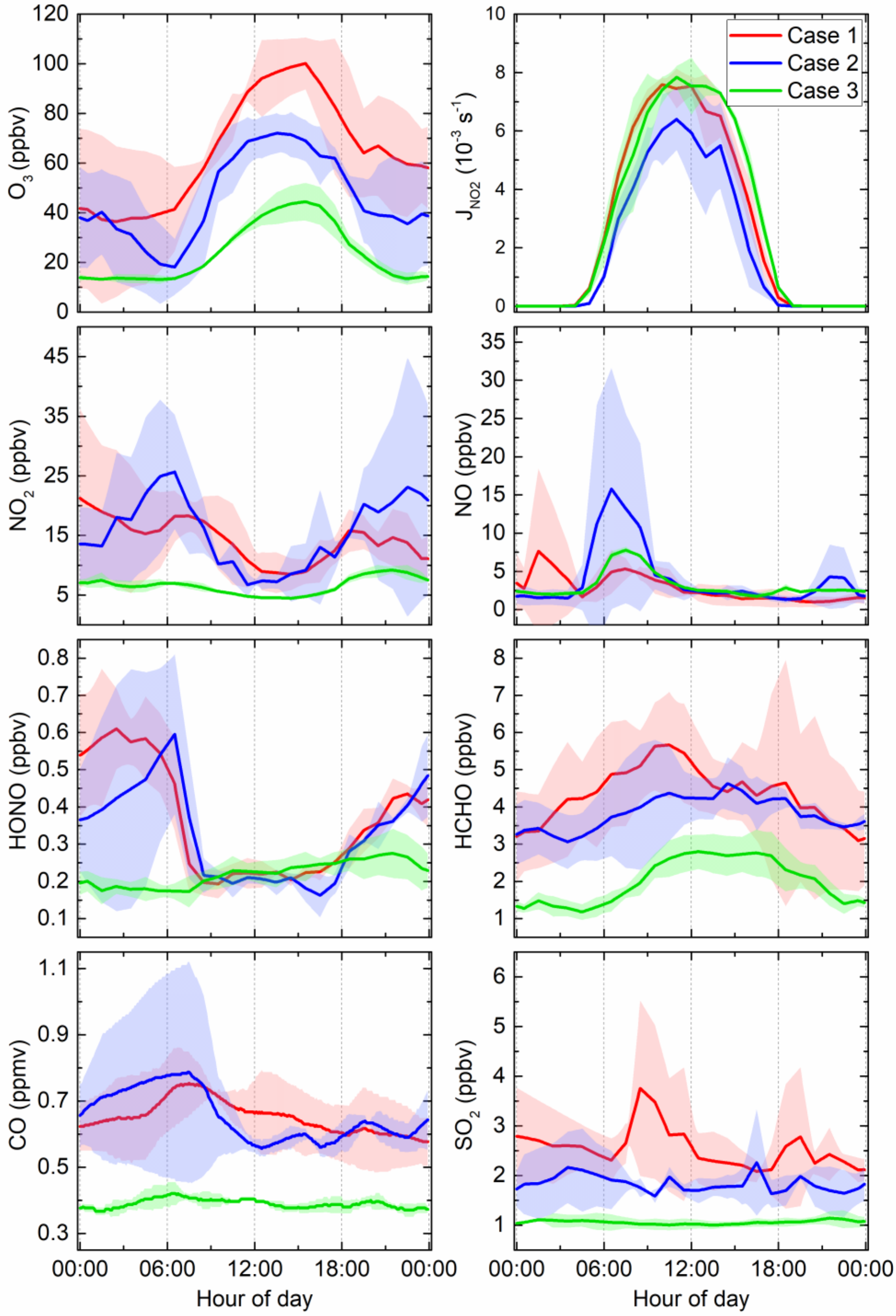

Figure S1. Mean diurnal profiles of measured trace gases mixing ratios for three cases. The shaded areas denote the standard deviation.

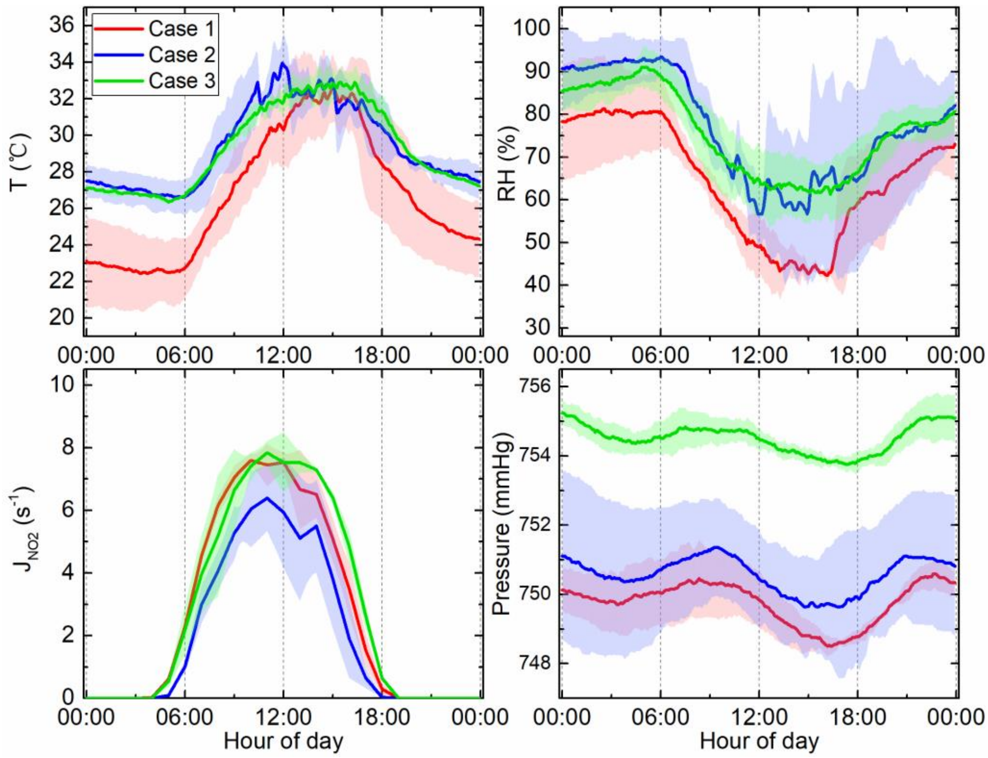

Figure S2. Mean diurnal profiles of meteorological parameters for three cases. The shaded areas denote the standard deviation.

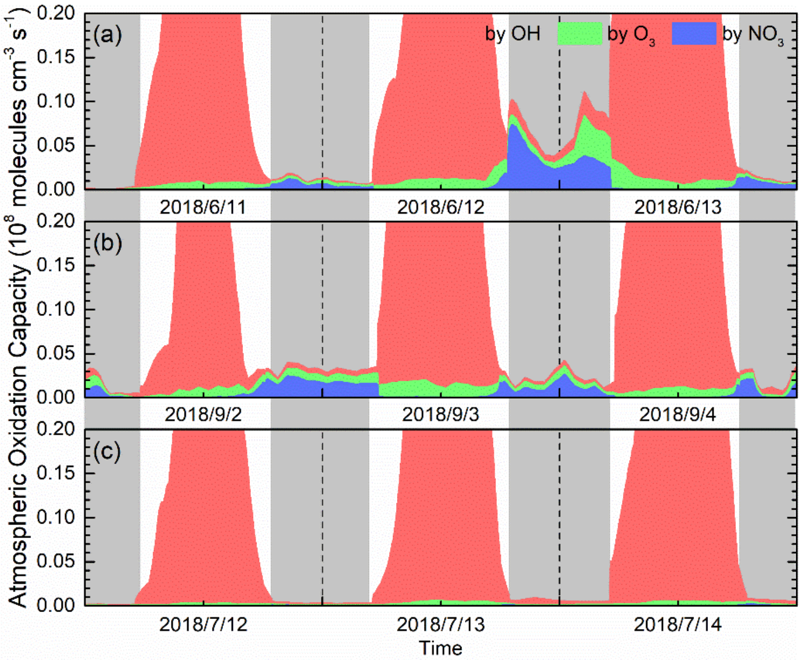

Figure S3. Modelled nighttime atmospheric oxidation capacity and contributions of major oxidants at an urban site of Shanghai during (a) Case 1, (b) Case 2 and (c) Case 3.

Simulated HO_x radical concentrations

Regarding the model-simulated concentrations of OH and HO_2, as shown in Figure S4, the maximum concentrations of OH for three cases were 9.97×10^6 molecule cm^{-3}, 8.34×10^6 molecule cm^{-3}, and 10.3×10^6 molecule cm^{-3}, respectively. And the maximum concentrations of HO_2 for three cases were 4.06×10^8 molecule cm^{-3}, 3.84×10^8 molecule cm^{-3}, and 3.41×10^8 molecule cm^{-3}, respectively. The previous simulated maximum concentrations of OH and HO_2 for urban site in Shanghai were 6.9×10^6 molecule cm^{-3} and 1.9×10^8 molecule cm^{-3} in summer, which lower than the simulated results here probably because of the different atmospheric conditions (Tan et al., 2019b). Due to lack of measured value of HO_x in Shanghai, we compared the measured value of other places in China. For instance, daily maximum concentrations were in the range of (4-17)$\times10^6$ molecule cm^{-3} for OH and (2–24)$\times10^8$ molecule cm^{-3} for HO_2 at the both suburban site Yufa and rural site Wangdu during summer in the North China Plain (Lu et al., 2013; Tan et al., 2017). In autumn, maximum median radical concentrations of 4.5×10^6 molecule cm^{-3} for OH at noon and 3×10^8 molecule cm^{-3} for HO_2 were reported for the Pearl River Delta in the early afternoon (Tan et al., 2019a). The simulated HO_x concentrations in this study were comparable with the measured results of other places in China, suggesting the moderate abundance of the HOx radical in Shanghai.

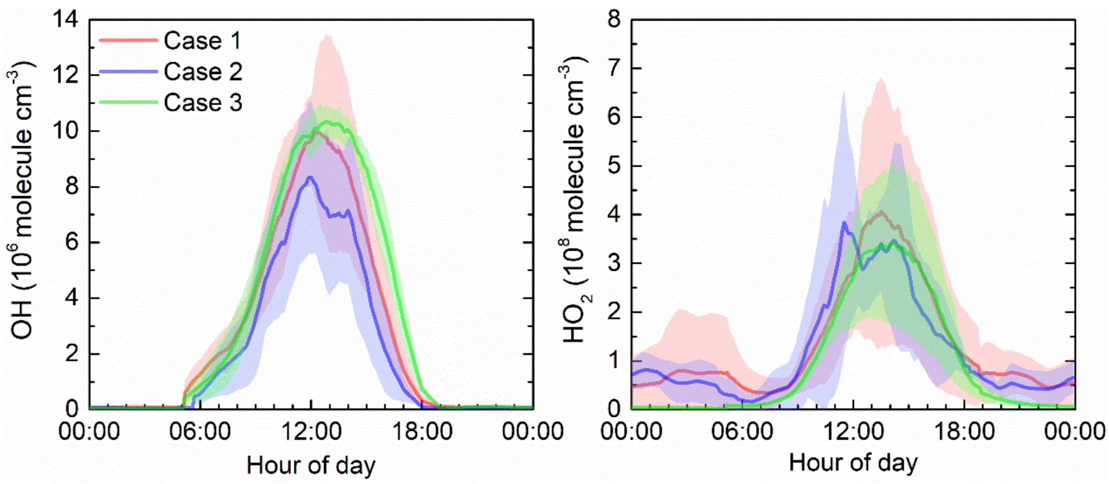

Figure S4. Mean diurnal profiles of the simulated HO_x concentrations in three cases in Shanghai. The shaded areas denote the standard deviation.

Impacts of deposition process in the simulation

We have conducted a simulation scenario considering the deposition process in order to discuss its impacts on intermediates. The loss of all unrestricted and model-generated species caused by the deposition is set as the accumulation of the deposition velocity of 0.01 m s^{-1} in the boundary layer (Santiago et al., 2016). Given that the boundary layer height (BLH) varied typically from 400 m at night to 1400 m in the afternoon during summer, which means that the lifetime of the model-generated species was ranged between ~11 h at night and ~40 h during the afternoon (Shi et al., 2015).

Afterwards, we have compared the simulated radical yields, AOC, OH reactivity, and OH chain length with or without considering the deposition process (see Table. S1). The simulated scenario without deposition is called Scenario N and the simulated scenario considering deposition is called Scenario Y. It can be clearly seen that the simulation results (OH, HO_2, RO_2, AOC, OH reactivity and OH chain length) without considering deposition term are enhanced to some extent compared with those with considering deposition term in three cases, especially for the intermediate (e.g. HO_2, RO_2), the results of Case 2 and Case 3 are increased by more than 50%. Therefore, it can be concluded that the deposition process has a great influence on the intermediates, which should be taken into account in the simulation.

Table S1. Summary of simulation results considering and not considering deposition process. All results are the average value of 06:00-18:00. N – Not considering deposition; Y – considering deposition.

Case 1	**OH** 10^6 mole cm^{-3}	**HO_2** 10^8 mole cm^{-3}	**RO_2** 10^8 mole cm^{-3}	**AOC** 10^8 mole cm^{-3} s^{-1}	**OH reactivity** s^{-1}	**OH chain length**
N	5.65±3.16	2.40±1.46	1.48±0.86	0.45±0.23	11.71±2.37	3.39±0.69
Y	5.27±3.13	1.99±1.29	1.09±0.70	0.42±0.22	11.48±2.16	3.17±0.63
(N-Y)/Y	7.21%	20.60%	35.78%	7.14%	2.00%	6.94%
Case 2	**OH** 10^6 mole cm^{-3}	**HO_2** 10^8 mole cm^{-3}	**RO_2** 10^8 mole cm^{-3}	**AOC** 10^8 mole cm^{-3} s^{-1}	**OH reactivity** s^{-1}	**OH chain length**
N	4.73±2.77	2.86±1.65	2.33±1.26	0.44±0.24	13.48±4.29	4.61±1.15
Y	4.05±2.68	1.87±1.18	1.34±0.82	0.37±0.22	12.86±3.80	3.75±0.90
(N-Y)/Y	16.79%	52.94%	73.88%	18.92%	4.82%	22.93%
Case 3	**OH** 10^6 mole cm^{-3}	**HO_2** 10^8 mole cm^{-3}	**RO_2** 10^8 mole cm^{-3}	**AOC** 10^8 mole cm^{-3} s^{-1}	**OH reactivity** s^{-1}	**OH chain length**
N	6.99±3.13	2.66±1.58	2.46±1.49	0.45±0.23	8.43±1.53	6.06±1.31
Y	6.12±3.37	1.76±1.22	1.51±1.08	0.40±0.23	8.41±1.21	4.96±1.08
(N-Y)/Y	14.22%	51.14%	62.91%	12.50%	0.24%	22.18%

Since the used deposition velocity and the BLH are empirical values from the previous literatures (Shi et al., 2015; Santiago et al., 2016), we have also carried out the sensitivity study on the deposition velocity and boundary layer height. The basic simulation scenario was set as deposition velocity of 0.01 m s^{-1} and the height of boundary layer varied from 400 m at night to 1400 m in the afternoon. Table S2 shows the settings of different simulation scenarios for the sensitivity study.

Table S2. Settings of simulation scenarios for sensitivity study.

Scenarios	deposition velocity (m s^{-1})	boundary layer-night (m)	boundary layer-noon (m)	Lifetime
Basic	0.01	400	1400	Night: 11 h; Day: 49 h
A	0.01	400	1000	Night: 11 h; Day: 28 h
B	0.01	400	2000	Night: 11 h; Day: 56 h
C	0.01	300	1400	Night: 8 h; Day: 39 h
D	0.01	500	1400	Night: 14 h; Day: 39 h
E	0.008	400	1400	Night: 14 h; Day: 49 h
F	0.012	400	1400	Night: 9 h; Day: 32 h

The sensitivity simulation results are summarized in Table S3, which demonstrated that the impacts of variations of deposition velocity and BLH on the modeling results were negligible (i.e. < 3% in OH, HO_2, RO_2, AOC, OH reactivity and OH chain length).

Table S3. Summary of model sensitivity test results

Case 1	**OH** 10^6 **mole cm^{-3}**	**HO_2** 10^8 **mole cm^{-3}**	**RO_2** 10^8 **mole cm^{-3}**	**AOC** 10^8 **mole cm^{-3} s^{-1}**	**OH reactivity** **s^{-1}**	**OH chain length**
Basic	5.27±3.13	1.99±1.29	1.09±0.70	0.42±0.22	11.48±2.16	3.17±0.63
A	5.26±3.12	1.97±1.27	1.07±0.68	0.42±0.22	11.46±2.16	3.16±0.62
B	5.28±3.13	2.01±1.29	1.11±0.71	0.42±0.22	11.49±2.16	3.17±0.63
C	5.25±3.13	1.97±1.28	1.07±0.69	0.42±0.22	11.44±2.13	3.16±0.63
D	5.29±3.12	2.01±1.29	1.11±0.70	0.42±0.22	11.50±2.18	3.17±0.62
E	5.30±3.12	2.02±1.29	1.12±0.71	0.42±0.22	11.51±2.18	3.18±0.62
F	5.25±3.12	1.97±1.28	1.07±0.69	0.42±0.22	11.45±2.14	3.16±0.63
(A-Basic)/Basic	-0.23%	-0.90%	-1.87%	-0.48%	-0.17%	-0.22%
(B-Basic)/Basic	0.21%	0.79%	1.64%	0.43%	0.15%	0.20%
(C-Basic)/Basic	-0.42%	-0.92%	-1.78%	-0.84%	-0.29%	-0.30%
(D-Basic)/Basic	0.33%	0.74%	1.45%	0.67%	0.23%	0.24%
(E-Basic)/Basic	0.46%	1.26%	2.54%	0.95%	0.33%	0.37%
(F-Basic)/Basic	-0.39%	-1.05%	-2.10%	-0.79%	-0.27%	-0.31%
Case 2	**OH** 10^6 **mole cm^{-3}**	**HO_2** 10^8 **mole cm^{-3}**	**RO_2** 10^8 **mole cm^{-3}**	**AOC** 10^8 **mole cm^{-3} s^{-1}**	**OH reactivity** **s^{-1}**	**OH chain length**
basic	4.05±2.68	1.87±1.18	1.34±0.82	0.37±0.22	12.86±3.80	3.75±0.90
A	4.04±2.68	1.84±1.16	1.31±0.80	0.37±0.22	12.83±3.80	3.73±0.90
B	4.07±2.69	1.89±1.19	1.37±0.83	0.37±0.22	12.89±3.80	3.75±0.90
C	4.02±2.68	1.84±1.17	1.31±0.81	0.36±0.22	12.80±3.76	3.73±0.90
D	4.08±2.68	1.89±1.19	1.37±0.83	0.37±0.22	12.92±3.83	3.76±0.90
E	4.09±2.69	1.91±1.20	1.38±0.84	0.37±0.22	12.94±3.83	3.77±0.90
F	4.03±2.68	1.84±1.16	1.31±0.80	0.36±0.22	12.81±3.77	3.73±0.90
(A-Basic)/Basic	-0.38%	-1.30%	-2.06%	-0.67%	-0.23%	-0.28%
(B-Basic)/Basic	0.35%	1.17%	1.85%	0.63%	0.21%	0.26%

(C-Basic)/Basic	-0.76%	-1.52%	-2.22%	-1.38%	-0.50%	-0.49%
(D-Basic)/Basic	0.62%	1.26%	1.84%	1.12%	0.40%	0.40%
(E-Basic)/Basic	0.86%	2.08%	3.13%	1.57%	0.55%	0.57%
(F-Basic)/Basic	-0.68%	-1.63%	-2.47%	-1.22%	-0.44%	-0.46%
Case 3	**OH** 10^6 **mole cm**$^{-3}$	**HO_2** 10^8 **mole cm**$^{-3}$	**RO_2** 10^8 **mole cm**$^{-3}$	**AOC** 10^8 **mole cm**$^{-3}$ **s**$^{-1}$	**OH reactivity** **s**$^{-1}$	**OH chain length**
basic	6.12±3.37	1.76±1.22	1.51±1.08	0.40±0.23	8.41±1.21	4.96±1.08
A	6.10±3.37	1.74±1.21	1.48±1.06	0.40±0.23	8.39±1.22	4.95±1.08
B	6.14±3.37	1.78±1.23	1.54±1.10	0.41±0.23	8.42±1.21	4.97±1.08
C	6.09±3.39	1.74±1.22	1.49±1.08	0.40±0.23	8.38±1.20	4.94±1.08
D	6.14±3.35	1.77±1.22	1.53±1.08	0.41±0.23	8.43±1.23	4.97±1.08
E	6.16±3.35	1.79±1.23	1.55±1.10	0.41±0.23	8.44±1.22	4.97±1.08
F	6.09±3.38	1.74±1.21	1.48±1.07	0.40±0.23	8.38±1.20	4.94±1.08
(A-Basic)/Basic	-0.30%	-1.44%	-2.08%	-0.59%	-0.25%	-0.20%
(B-Basic)/Basic	0.26%	1.22%	1.76%	0.52%	0.20%	0.18%
(C-Basic)/Basic	-0.47%	-0.93%	-1.30%	-0.85%	-0.37%	-0.28%
(D-Basic)/Basic	0.38%	0.79%	1.10%	0.70%	0.28%	0.23%
(E-Basic)/Basic	0.56%	1.60%	2.28%	1.05%	0.43%	0.35%
(F-Basic)/Basic	-0.46%	-1.33%	-1.90%	-0.85%	-0.36%	-0.28%

Finally, the basic simulation scenario of deposition velocity of 0.01 m s^{-1} and the height of boundary layer varied from 400 m at night to 1400 m in the afternoon was used in the simulation for the three cases study. And the relevant simulated results and discussion were replaced in the manuscript.

The impacts of cloud cover on J_{NO_2} and J_{O^1D}

The impacts of cloud cover on J_{NO_2} and J_{O^1D} are considerable complex. Crawford et al. (2003) reported that the observed UV actinic flux under cloudy conditions that unoccluded the sun disk is 40% higher than the clear sky value. When the solar disk is occluded, reductions in actinic flux appear to vary inversely with cloud fraction in some instances. In the broken cloud field, the fluctuation ranges of J_{O^1D} and J_{NO_2} are different, and the change of J_{NO_2} is larger than that of J_{O^1D}. Monks et al. (2004) research also revealed that the photolysis frequencies in the UVB and UVA do not vary linearly under different atmospheric conditions in a cloudy field. Cloud cover and its quantitative effects on UVA and UVB are important for the correction of J_{O^1D} from the measured J_{NO_2} scaling. Whalley et al. (2018) used the ratio of the model calculated J_{O^1D} in the clear sky to the observed J_{O^1D} to account for clouds and to determine photolysis rates of other photolabile species.

Since we have not measured J_{O^1D} but only for J_{NO_2}, we are not able to use this method to determine cloud cover. However, we try to seek an approximate quantitative relationship between the fluctuation magnitude of J_{NO_2} and J_{O^1D} in cloudy days compared to clear sky:

$$\%\ \text{reduction or enhancement } in\ j(X) = \left(\frac{j(X)_{clear} - j(X)_{cloudy}}{j(X)_{clear}}\right) \times 100 \qquad \text{(E1)}$$

$$\%j(O^1D) \approx 1.08\%j(NO_2) - 0.12 \qquad \text{(E2)}$$

Where $\%j(O^1D)$ and $j(NO_2)$ is calculated by the equation (E1). Please note that the equation E2 here is an approximate relationship between $\%j(O^1D)$ and $\%j(NO_2)$ on a certain summer day in the study by Monks et al. (2004).

In addition, it is also necessary to correct the cloudy day values of J_{O^1D} considering the changes in overhead ozone column between the cloudy and clear day. The ratio of the overhead ozone column of clear sky day to that of cloudy day is used as the calibration coefficient k. The J_{O^1D} of cloudy day can be calculated by equation (E3):

$$j(O^1D)_{cloud} = kj(O^1D)_{clear}\left(1 - \%j(O^1D)\right) \qquad \text{(E3)}$$

Table S4 lists the overhead total ozone column and calibration coefficient k for three cases, in which total ozone column data taken from OMI (download from https://disc.gsfc.nasa.gov/datasets/OMDOAO3_003/summary) and taken for 121.51°E, 31.34°N with a radius of 20 km at 13:45 local overpass time. The OMI data from September 2nd to 4th are missing due to no data available after the filtering (filtering conditions: solar zenith angles < 70°, cloud cover < 0.5, pixels were not affected by the row anomaly are used), and we took the mean value of available total ozone column from May to October as the reference data (294.262±18.240 DU). Considering that the total column concentration was relatively low in September, the final total ozone column of 290.000 DU was used.

Table S4. Daily ozone total column for three cases in Shanghai. Data taken from OMI. NOTE: Missing data on September 2, 3 and 4.

	Date	O_3 total column/DU	k
Case 1	11-Jun	341.955	0.874
	12-Jun	319.755	0.935
	13-Jun	321.510	0.929
Case 2	2-Sep	*290.000*	*1.030*

	3-Sep	*290.000*	*1.030*
	4-Sep	*290.000*	*1.030*
Case 3	12-Jul	277.529	1.077
	13-Jul	299.974	0.996
	14-Jul (clear sky)	298.841	1.000

In this study, we have used the observed J_{NO_2} data and the J_{O^1D} data scaled by J_{NO_2}. As shown in Figure S5, it is a clear sky on July 14, 2018 in Case 3. The J_{NO_2} on this day and the J_{O^1D} obtained by scaling J_{NO_2} can be considered as real or 'measured' $j(X)_{clear}$. The images of sky conditions for the remaining days of these three cases are shown in Figure S6 (the images on July 12 are missing).

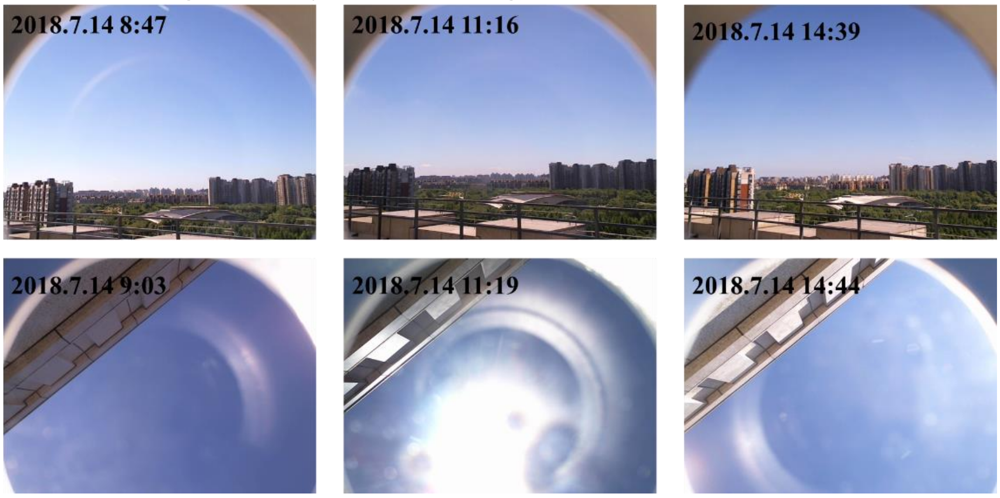

Figure S5. Sky images on July 14, 2018

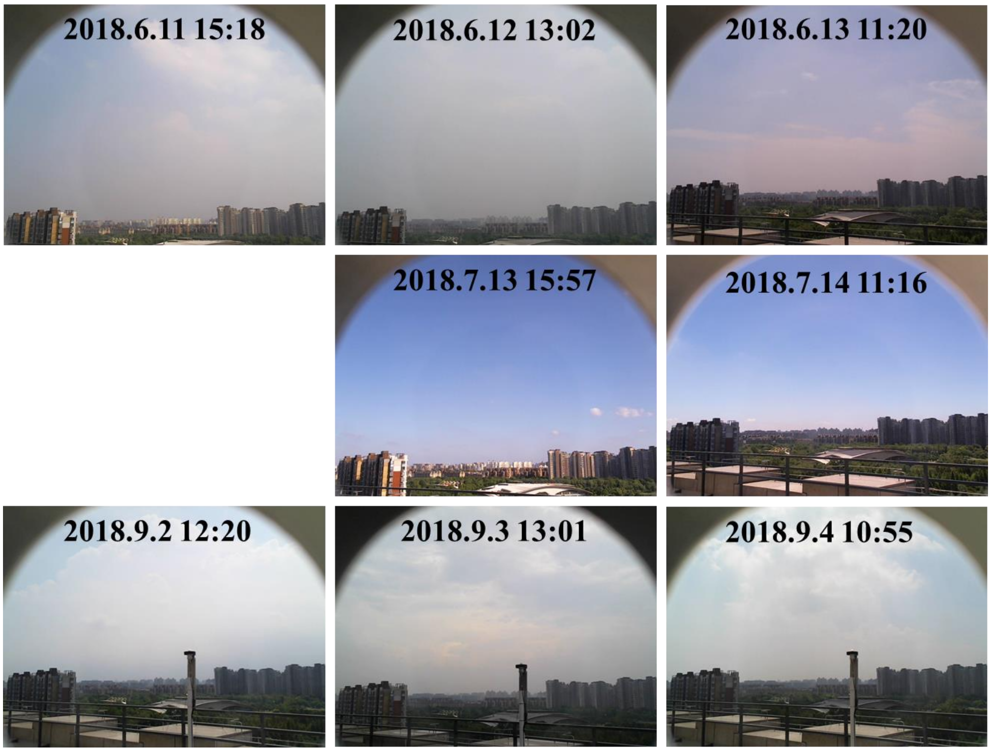

Figure S6. Representative sky images in three cases

Therefore, we can determine $\%j(NO_2)$ by the difference between J_{NO2} on clear sky and cloudy days, and then calculate the $J_{O1Dcloudy}$ via equation (E3). Figure S7 shows the difference of calibrated J_{O1D} and J_{O1D} without calibration for clouds in three cases. Compared with the J_{O1D} scaled by the measured J_{NO2} directly, the calibrated J_{O1D} of the three cases changed by -0.75%, 32.22%, and 7.97%, respectively.

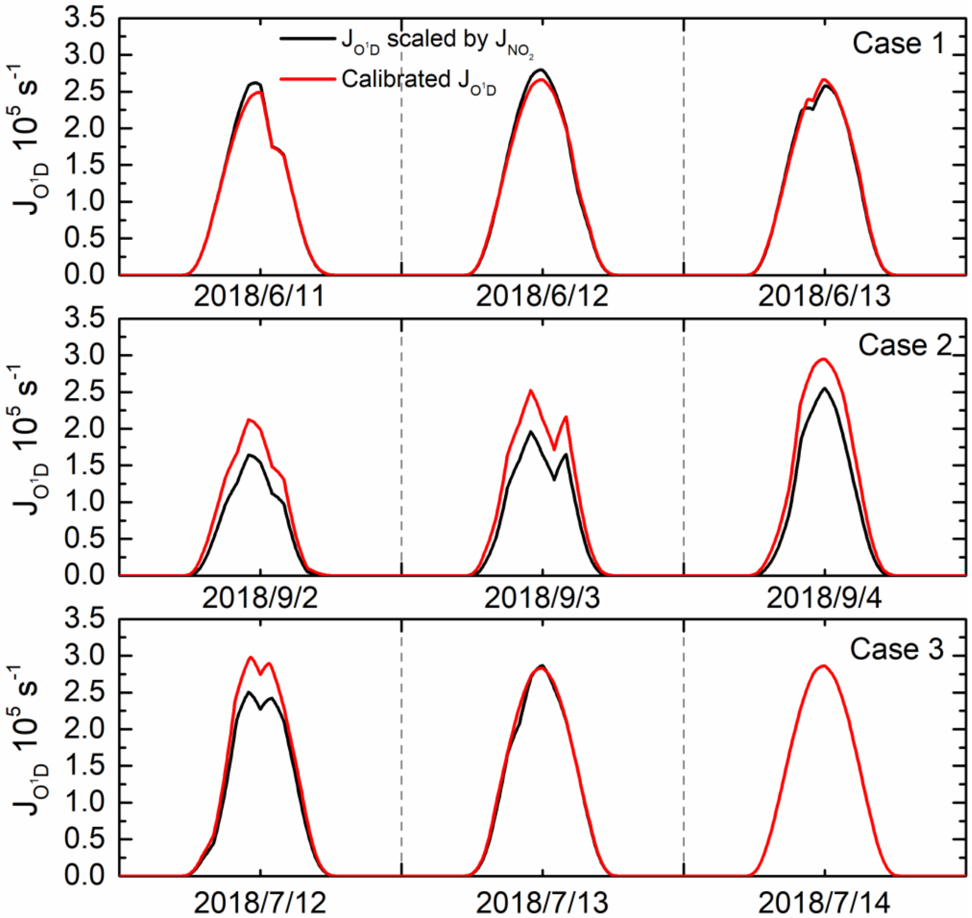

Figure S7. Comparison of calibrated J_{O1D} for cloud cover and J_{O1D} without calibration scaled directly by J_{NO2} in three cases

Then, we have ran the simulation scenarios G with the calibrated J_{O1D} and compared the results with simulation scenarios Basic, as listed in Table S5. The impact of J_{O1D} on the simulation results of Case 1 was negligible, and the impact on the simulation results of Case 3 was less than 3%. In Case 2 with the largest change in J_{O1D}, the effects on radicals and AOC were less than 10%, and the effects on OH reactivity and OH chain length could be ignored.

Table S5. Summary of simulation results with or without J_{O1D} calibration

Case 1 Scenarios	**J_{O1D}** 10^{-5} s^{-1}	**OH** 10^6 mole cm^{-3}	**HO_2** 10^8 mole cm^{-3}	**RO_2** 10^8 mole cm^{-3}	**AOC** 10^8 mole cm^{-3} s^{-1}	**OH reactivity** s^{-1}	**OH chain length**
Basic	1.32±0.93	5.28±3.12	1.99±1.28	1.09±0.70	0.42±0.22	11.48±2.16	3.17±0.63
G	1.31±0.90	5.26±3.10	1.99±1.29	1.09±0.70	0.42±0.22	11.48±2.16	3.17±0.63
Discrepancy	-0.75%	-0.40%	0	0	0	0	0
Case 2	**J_{O1D}**	**OH**	**HO_2**	**RO_2**	**AOC**	**OH reactivity**	**OH chain**

Scenarios	10^{-5} s^{-1}	10^6 mole cm^{-3}	10^8 mole cm^{-3}	10^8 mole cm^{-3}	10^8 mole cm^{-3} s^{-1}	s^{-1}	length
Basic	0.90±0.72	4.06±2.68	1.88±1.18	1.35±0.82	0.37±0.22	12.96±3.89	3.77±0.89
G	1.19±0.89	4.41±2.94	2.03±1.29	1.46±0.89	0.40±0.24	12.84±3.80	3.74±0.89
Discrepancy	32.22%	8.62%	7.98%	8.15%	8.11%	-0.93%	-0.80%
Case 3 Scenarios	**J_{O1D}** 10^{-5} s^{-1}	**OH** 10^6 mole cm^{-3}	**HO_2** 10^8 mole cm^{-3}	**RO_2** 10^8 mole cm^{-3}	**AOC** 10^8 mole cm^{-3} s^{-1}	**OH reactivity** s^{-1}	**OH chain length**
Basic	1.40±0.97	6.13±3.36	1.76±1.22	1.51±1.08	0.40±0.23	8.41±1.21	4.96±1.08
G	1.49±0.97	6.22±3.44	1.78±1.23	1.53±1.09	0.41±0.24	8.41±1.21	4.95±1.08
Discrepancy	7.98%	1.47%	1.14%	1.32%	2.50%	0	-2.02%

Based on the discussion above, it is found that the calibrated J_{O1D} considering clouds condition deviated from the J_{O1D} directly scaled by the measured J_{NO2} for -0.75%, 32.22%, and 7.97% during these three cases. Additionally, the modelling results shows the limited impacts of J_{O1D} calibration for clouds on the results and has not changed the main conclusions for the three cases in this study.

Due to the particularity in the approximation method of equation (E2) and uncertainty on ozone column data, we think this calibration method is not an accurate way to calibrate J_{O1D} for this study. Therefore, we decided to use the J_{O1D} scaled by the measured J_{NO2} as the O_3 photolysis frequency in three cases.

References

Crawford, J., Shetter, R. E., Lefer, B., Cantrell, C., Junkermann, W., Madronich, S., and Calvert, J.: Cloud impacts on UV spectral actinic flux observed during the International Photolysis Frequency Measurement and Model Intercomparison (IPMMI), J. Geophys. Res., 108, https://doi.org/10.1029/2002jd002731, 2003.

Lu, K. D., Hofzumahaus, A., Holland, F., Bohn, B., Brauers, T., Fuchs, H., Hu, M., Häseler, R., Kita, K., Kondo, Y., Li, X., Lou, S. R., Oebel, A., Shao, M., Zeng, L. M., Wahner, A., Zhu, T., Zhang, Y. H., and Rohrer, F.: Missing OH source in a suburban environment near Beijing: observed and modelled OH and HO2 concentrations in summer 2006, Atmos. Chem. Phys., 13, 1057-1080, https://doi.org/10.5194/acp-13-1057-2013, 2013.

Monks, P. S., Rickard, A. R., and Hall, S. L.: Attenuation of spectral actinic flux and photolysis frequencies at the surface through homogenous cloud fields, J. Geophys. Res., 109, https://doi.org/10.1029/2003jd004076, 2004.

Santiago, J.-L., Martilli, A., and Martin, F.: On dry deposition modelling of atmospheric pollutants on vegetation at the microscale: Application to the impact of street vegetation on air quality, Boundary Layer Meteorol., 162, 451-474, https://doi.org/10.1007/s10546-016-0210-5, 2016.

Shi, C., Wang, S., Liu, R., Zhou, R., Li, D., Wang, W., Li, Z., Cheng, T., and Zhou, B.: A study of aerosol optical properties during ozone pollution episodes in 2013 over Shanghai, China, Atmos. Res., 153, 235-249, https://doi.org/10.1016/j.atmosres.2014.09.002, 2015.

Tan, Z., Fuchs, H., Lu, K., Hofzumahaus, A., Bohn, B., Broch, S., Dong, H., Gomm, S., Häseler, R., He, L., Holland, F., Li, X., Liu, Y., Lu, S., Rohrer, F., Shao, M., Wang, B., Wang, M., Wu, Y., Zeng, L., Zhang, Y., Wahner, A., and Zhang, Y.: Radical chemistry at a rural site (Wangdu) in the North China Plain: observation and model calculations of OH, HO2 and RO2 radicals, Atmos. Chem.

Phys., 17, 663-690, https://doi.org/10.5194/acp-17-663-2017, 2017.

Tan, Z., Lu, K., Hofzumahaus, A., Fuchs, H., Bohn, B., Holland, F., Liu, Y., Rohrer, F., Shao, M., Sun, K., Wu, Y., Zeng, L., Zhang, Y., Zou, Q., Kiendler-Scharr, A., Wahner, A., and Zhang, Y.: Experimental budgets of OH, HO_2, and RO_2 radicals and implications for ozone formation in the Pearl River Delta in China 2014, Atmos. Chem. Phys., 19, 7129-7150, https://doi.org/10.5194/acp-19-7129-2019, 2019a.

Tan, Z., Lu, K., Jiang, M., Su, R., Wang, H., Lou, S., Fu, Q., Zhai, C., Tan, Q., Yue, D., Chen, D., Wang, Z., Xie, S., Zeng, L., and Zhang, Y.: Daytime atmospheric oxidation capacity in four Chinese megacities during the photochemically polluted season: a case study based on box model simulation, Atmos. Chem. Phys., 19, 3493-3513, https://doi.org/10.5194/acp-19-3493-2019, 2019b.

Whalley, L. K., Stone, D., Dunmore, R., Hamilton, J., Hopkins, J. R., Lee, J. D., Lewis, A. C., Williams, P., Kleffmann, J., Laufs, S., Woodward-Massey, R., and Heard, D. E.: Understanding in situ ozone production in the summertime through radical observations and modelling studies during the Clean air for London project (ClearfLo), Atmos. Chem. Phys., 18, 2547-2571, https://doi.org/10.5194/acp-18-2547-2018, 2018.